State observer to improve the VSG control stability

Audrey Moulichon, Mazen Alamir, Lauric Garbuio, Vincent Debusschere, Mustapha Amine Rahmani, Cédric Boudinet, William Noris, Nouredine Hadjsaid

State observer to improve the VSG control stability

Audrey Moulichon*†‡, Mazen Alamir†, Lauric Garbuio*, Vincent Debusschere*, Mustapha Amine Rahmani‡, Cédric Boudinet*, William Noris* and Nouredine Hadjsaid*
*Univ. Grenoble Alpes, CNRS, Grenoble INP, G2ELab, F-38000 Grenoble, France
†Univ. Grenoble Alpes, CNRS, Grenoble INP, Gipsa-lab, F-38000 Grenoble, France
‡Schneider Electric Industries, Power Conversion department, 38000 Grenoble, France
Emails: audrey.moulichon@gmail.com and vincent.debusschere@grenoble-inp.fr

***Abstract*—This paper proposes an observer-based current controller for a virtual synchronous generators (VSG) to improve its operational performances. First, the model and the controllers are analytically described. Two controller are compared to the proposed one (PI integrating a state observer): a traditional PI and a PI integrating virtual impedances for filtering. Secondly, the advantage of the observer in the current controller loop for the VSG application is studied and compared to the other controllers. Finally, experimental results validate the capacity of the VSG-based inverter to supply unknown and unpredictable loads, thanks to the integration of the observer in the current control loop.**

***Index Terms*—Grid Forming Inverters, State Observer, Microgrids, Power Generation, Renewable Energies, State-Space model, Synchronous Machine, Synchronverter, Virtual Synchronous Generator**

Nomenclature

Symbol	Definition
ω_r and ω_0	Machine rotor electrical angular velocity and its base value, $\omega_r = \omega_{rotor}/\omega_0$
i_d and i_q	Machine *dq* stator output current
V_{DC}	Inverter input DC voltage
α_d and α_q	*dq* inverter output duty ratio
V_i, V_i^d and V_i^q	Unifilar and *dq* inverter voltage considering: $V_i = \alpha.\frac{V_{DC}}{2}$
E, e^d and e^q	Single-line and *dq* filter voltage
V_g, V_g^d and V_g^q	Single-line and *dq* grid voltage
i_L, i_L^d and i_L^q	Single-line and *dq* output inverter current
i_g, i_g^d and i_g^q	Single-line and *dq* grid inverter current
L_L and R_L	Inverter's inductance and resistor
L_g and R_g	Grid's inductance and resistor
C_f and R_f	Capacitive filter's inductance and resistor

Notation

$\mathbb{I}_n$	Eye matrix of size n
$\mathbb{O}_{i,j}$	Full zeros matrix of i rows and j colons
$\mathbb{M}_{i,j}$	Matrix of i rows and j colons
$\boldsymbol{M}^\intercal$	Transposed matrix of $\boldsymbol{M}$
$\boldsymbol{M}^s$	Discrete state space model of $\boldsymbol{M}$
$\hat{\boldsymbol{M}}$	Observed vectors or system
$\boldsymbol{M}^+$	Next step state-space value of $\boldsymbol{M}$
$\overline{\boldsymbol{M}}$	Extended state vector of $\boldsymbol{M}$

I. Introduction

The microgrids have received substantial attention as possible relevant solution for integration renewable energy sources (RES), for allowing the energy access to remote locations and also ensuring a potential increase of the system resiliency and reliability. Indeed, in recent years, the traditional distributed energy resources (DER) supplying energy to microgrids (usually diesel generator-sets) are supplanted by supplier based on RES. However, their intermittency leads to major stability issues, especially in the context of microgrids, notably because these sources usually decrease the available inertia of an already weak grid [1]. Hence, the traditional control strategies for inverters, interfacing the various DERs connected to the microgrid, needs adapting.

The virtual synchronous generator (VSG) is one of the most popular solution that can participate in increasing the microgrids inertia and also easily be integrated into traditional stability studies because it presents similarities with an actual synchronous machine [2], [3]. Various projects have shown the advantages of VSG for the insertion of renewable energy source in microgrids [4], [5]. Other researches emerge with various topologies, based for instance on a simplified [6], [7] or an algebraic model [8], [9].

The most frequently used solution is a multi-loop control architecture that implements three regulations, namely on current, voltage and frequency [10], [11]. The controllers are developed to both increase the performances of the VSG in terms of capacity to follow the reference of the model of the synchronous machine and to minimize the creation of oscillations at the output of the inverter. The oscillations are caused partly by resonances occurring after the grid's frequency which then destabilize the controlled system [12]. To that end, we can cite for example the integration of a proportional integrator (PI) and a resonant regulators [13], a robust H_∞ method [14] or a fuzzy controller [15].

To the best of our knowledge, the use of an observer has not been considered in the controller of a VSG. The solution proposed in this paper is a combination of a PI controller and an observer to improve the performances of the VSG, in terms of rapidity and stability during load impacts, and avoid resonances thanks to the reconstruction of the characteristics of the load by the observer.

In this paper, the first part details the model used to represent the grid-connected inverter. Then, based on this model, the proposed controller of the VSG is analytically described considering the addition of a state-space observer. Then, in a second part, the improvement due to the observer are highlighted with an analytical analysis. Finally, in the last section, experimental results are shown to validate the operational behavior of the proposed control architecture for

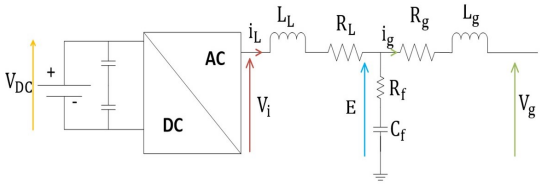

Fig. 1. Single-line inverter's connection to the grid.

TABLE I
INVERTER PARAMETERS.

Parameter	Values	Unit
L_L	870 e^3	H
R_L	7.1 e^3	Ω
L_g	60 e^3	H
R_g	10 e^3	Ω
C_f	152 e^{-6}	F
R_f	10 e^3	Ω

a VSG considering the integration of the state-space observer.

II. Models For The VSG Controller

The model of the inverter is expressed in the *dq*-frame and in per unit (p.u.). The synchronous machine model reference in the VSG-based inverter has been extracted from [16] and is based on initial developments presented in [17]. In addition, as the proposed current controller has been developed using a state-space model, any other model of synchronous machine can be implemented, for instance just the swing equation if ever only virtual inertia is needed.

A. Grid Connected Inverter

Fig. 1 and Table I detail the parameters used to model the inverter and its connection to the grid. The inverter's resistor R_L, the resistor of the capacitive filter R_f and the grid line resistor R_g are not neglected. Hence, a RL-RC-RL output inverter filter is preferred for an increased accuracy instead of the traditionally used LCL output filter. The inverter's outputs are defined in the *dq*-frame in (1).

$$\begin{cases} \frac{de^d}{dt} = \omega_0 \left(\omega_r.e^q + \frac{i_L^d - i_g^d}{C_f} - \frac{R_f.R_L}{L_L}.i_L^d + \frac{R_f.R_g}{L_g}.i_g^d \right. \\ \qquad \left. + \frac{R_f}{L_L}.V_i^d + \frac{R_f}{L_g}.V_g^d - e^d.R_f \left(\frac{1}{L_L} + \frac{1}{L_g} \right) \right) \\ \frac{de^q}{dt} = \omega_0 \left(-\omega_r.e^d + \frac{i_L^q - i_g^q}{C_f} - \frac{R_f.R_L}{L_L}.i_L^q + \frac{R_f.R_g}{L_g}.i_g^q \right. \\ \qquad \left. + \frac{R_f}{L_L}.V_i^q + \frac{R_f}{L_g}.V_g^q - e^q.R_f \left(\frac{1}{L_L} + \frac{1}{L_g} \right) \right) \end{cases} \tag{1}$$

B. State-space Model

To simplify and express (1) in a state-space framework, we assume that $\omega_r = 1$. This assumption is relevant since the dynamic frequency variations of the microgrid is limited to less than 10 % of the nominal value. This leads to the following state-space model of (2).

$$\dot{\boldsymbol{X}}_{SYS} = \boldsymbol{A}.\boldsymbol{X}_{SYS} + \boldsymbol{B}.\boldsymbol{U}_{SYS} + \boldsymbol{G}.\boldsymbol{W}_{SYS} \tag{2}$$

Where $\boldsymbol{X}_{SYS}$ represents the state vector, $\boldsymbol{U}_{SYS}$ the manipulated inputs and $\boldsymbol{W}_{SYS}$ the exogenous inputs defined in (3). The matrices $\boldsymbol{A}$, $\boldsymbol{B}$ and $\boldsymbol{G}$, based on the above inverter's models are proposed in Appendix.

$$\boldsymbol{X}_{SYS} = \begin{bmatrix} i_L^d \\ i_L^q \\ e^d \\ e^q \\ i_g^d \\ i_g^q \end{bmatrix}; \boldsymbol{U}_{SYS} = \begin{bmatrix} V_i^d \\ V_i^q \end{bmatrix}; \boldsymbol{W}_{SYS} = \begin{bmatrix} V_g^d \\ V_g^q \end{bmatrix} \tag{3}$$

For a model that can be easily implemented in an industrial card, a discrete-time version of the above state-space model is used and defined in (4).

$$\boldsymbol{X}_{SYS}^{+} = \boldsymbol{A}^s.\boldsymbol{X}_{SYS} + \boldsymbol{B}^s.\boldsymbol{U}_{SYS} + \boldsymbol{G}^s.\boldsymbol{W}_{SYS} \tag{4}$$

Where $\boldsymbol{X}_{SYS}^{+}$ represents the next state-space value of the vector $\boldsymbol{X}_{SYS}$. The matrices $\boldsymbol{A}^s$, $\boldsymbol{B}^s$ and $\boldsymbol{G}^s$ are the discrete state-space matrices of the continuous state-space model, defined in (2).

III. Designing The Controller Of The VSG

The objective of the current controller is to follow the reference currents defined by the synchronous machine model in various configurations of load variations. The current controller solution can be divided in two parts: the observer and the controller [18]. Thanks to the observer, the output load is reconstructed while the current controller uses the estimated load and the reference to choose the values of the manipulated variables, helping to supply the necessary output currents to the load should the estimation of the latter be correct.

A. Current Controller

The current controller has to force the inverter output currents i_L^d and i_L^q to follow the synchronous machine model current references, noted i^d and i^q, by providing the duty ratios to the inverter, α^d and α^q. In this section, the analytic PI controller model, previously used in [17], is described, based on the previous state-space model.

The controller's output, noted $\boldsymbol{\varepsilon}$, is the difference between the inverter's currents , i_L^d and i_L^q, and the references, the currents i_d and i_q. Hence, the output $\boldsymbol{\varepsilon}$ is defined in (5).

$$\boldsymbol{\varepsilon} = \begin{bmatrix} i_d - i_L^d \\ i_q - i_L^q \end{bmatrix} = \begin{bmatrix} i_d \\ i_q \end{bmatrix} + \boldsymbol{C}^s.\boldsymbol{X}_{SYS}; \quad \text{With } \boldsymbol{C}^s = -\begin{bmatrix} \mathbb{I}_2 & \mathbb{O}_{2,4} \end{bmatrix} \tag{5}$$

The state-space integrator, noted $\boldsymbol{\varepsilon}_{PI}$, is considered added to the current controller with the dynamics expressed in (6).

$$\boldsymbol{\varepsilon}_{PI}^{+} = \boldsymbol{\varepsilon}_{PI} + \boldsymbol{\varepsilon} \tag{6}$$

The controlled inverter duty ratio in the *dq*-axis and p.u. is defined in (7), where $\boldsymbol{K}_p$ and $\boldsymbol{K}_i$ are the controller's parameters, $\boldsymbol{K}_p \in \mathbb{M}_{2,2}$ and $\boldsymbol{K}_i \in \mathbb{M}_{2,2}$.

$$\begin{bmatrix} \alpha^d \\ \alpha^q \end{bmatrix} = \frac{2}{V_{DC}}. \begin{bmatrix} V_i^d \\ V_i^q \end{bmatrix} = \frac{2}{V_{DC}}. \left(\begin{bmatrix} e^d \\ e^q \end{bmatrix} + \boldsymbol{K}_p.\boldsymbol{\varepsilon} + \boldsymbol{K}_i.\boldsymbol{\varepsilon}_{PI} \right) \tag{7}$$

Hence, considering (2), (6) and (7), the PI controller model is detailed in (8).

$$\begin{bmatrix} \boldsymbol{X}_{SYS} \\ \boldsymbol{\varepsilon}_{PI} \end{bmatrix}^{+} = \begin{bmatrix} \boldsymbol{A}^s + \boldsymbol{K}_p.\boldsymbol{B}^s.\boldsymbol{C}^s & \boldsymbol{K}_i.\boldsymbol{B}^s \\ \boldsymbol{K}_p.\boldsymbol{C}^s & \mathbb{I}_{2,2} \end{bmatrix} . \begin{bmatrix} \boldsymbol{X}_{SYS} \\ \boldsymbol{\varepsilon}_{PI} \end{bmatrix} + \begin{bmatrix} \boldsymbol{G}^s \\ \mathbb{O}_{2,2} \end{bmatrix} . \boldsymbol{W}_{SYS} + \begin{bmatrix} (\boldsymbol{K}_p + \boldsymbol{K}_i).\boldsymbol{B}^s \\ \mathbb{I}_{2,2} \end{bmatrix} . \begin{bmatrix} i^d \\ i^q \end{bmatrix}$$

$$\begin{bmatrix} \alpha^d \\ \alpha^q \end{bmatrix} = \frac{2.\left[\begin{bmatrix} \mathbb{O}_{2,2} & \mathbb{I}_{2,2} & \mathbb{O}_{2,2} \end{bmatrix} + \boldsymbol{K}_p.\boldsymbol{C}^s \quad \boldsymbol{K}_i\right]}{V_{DC}} . \begin{bmatrix} \boldsymbol{X}_{SYS} \\ \boldsymbol{\varepsilon}_{PI} \end{bmatrix} + \frac{2.(\boldsymbol{K}_p + \boldsymbol{K}_i)}{V_{DC}} . \begin{bmatrix} i^d \\ i^q \end{bmatrix} \quad (8)$$

B. State-space Observer

The objective of the observer is to reconstruct, based on the available measures, the load variations at the output of the filter, characterized by the grid output voltages, V_g^d and V_g^q, and the grid output currents, i_g^d and i_g^q. The output inverter currents, i_L^d and i_L^q, and voltages e^d and e^q, are also measured by dedicated sensors.

As the load is not represented by a model but by its current and its voltage, the state observer model is true and not impacted by the characteristics of the load connected to the output of the controlled system.

The outputs vector $\boldsymbol{Y}$, aggregating all measurements, is defined as $\boldsymbol{Y} = \begin{bmatrix} i_L^d & i_L^q & e^d & e^q \end{bmatrix}^\intercal$. The linear combination of the state and input vectors is expressed in (9).

$$\boldsymbol{Y} = \boldsymbol{C}_{obs}^s.\boldsymbol{X}_{SYS}; \text{ with } \boldsymbol{C}^s = \begin{bmatrix} \mathbb{I}_4 & \mathbb{O}_{4,2} \end{bmatrix} \quad (9)$$

The exogenous input $\boldsymbol{W}_{SYS}$ is considered as a constant during multiple periods, so we have $\boldsymbol{W}_{SYS}^+ = \boldsymbol{W}_{SYS}$. The model considered for the discrete observer is detailed in (10).

$$\begin{cases} \overline{\boldsymbol{X}}^+ = \overline{\boldsymbol{A}}^s.\overline{\boldsymbol{X}} + \overline{\boldsymbol{B}}^s.\boldsymbol{U}_{SYS} \\ \boldsymbol{Y} = \overline{\boldsymbol{C}}^s.\ \overline{\boldsymbol{X}} \end{cases}$$
$$\text{With: } \overline{\boldsymbol{X}} = \begin{bmatrix} \boldsymbol{X}_{SYS} \\ \boldsymbol{W}_{SYS} \end{bmatrix}; \overline{\boldsymbol{A}}^s = \begin{bmatrix} \boldsymbol{A}^s & \boldsymbol{G}^s \\ \mathbb{O}_{2,6} & \mathbb{I}_2 \end{bmatrix};$$
$$\overline{\boldsymbol{B}}^s = \begin{bmatrix} \boldsymbol{B}^s \\ \mathbb{O}_{2,2} \end{bmatrix} \text{ and } \overline{\boldsymbol{C}}^s = \begin{bmatrix} \boldsymbol{C}_{obs}^s & \mathbb{O}_{4,2} \end{bmatrix} \quad (10)$$

Fortunately, the new extended model is observable considering the inverter parameters presented in Table I. Therefore, it is possible to compute a matrix gain $\boldsymbol{L}$ of a linear state observer, $\boldsymbol{L} \in \mathbb{M}_{8,2}$, expressed in (11).

$$\begin{cases} \hat{\overline{\boldsymbol{X}}}^+ = \left(\overline{\boldsymbol{A}}^s - \boldsymbol{L}.\overline{\boldsymbol{C}}^s\right).\hat{\overline{\boldsymbol{X}}} + \overline{\boldsymbol{B}}^s.\boldsymbol{U}_{SYS} + \boldsymbol{L}.\boldsymbol{Y} \\ \hat{\boldsymbol{Y}} = \overline{\boldsymbol{C}}^s.\hat{\overline{\boldsymbol{X}}} \end{cases} \quad (11)$$

C. Controller Integrating An Observer

The concatenation of the current controller model, expressed in (8), and the observer model, expressed in (11), provides the PI controller integrating a state-space observer, defined in (12).

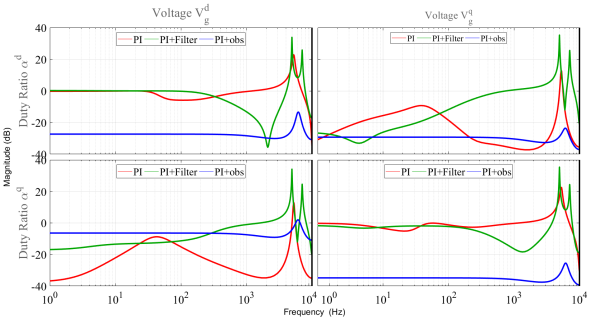

(a) Magnitude

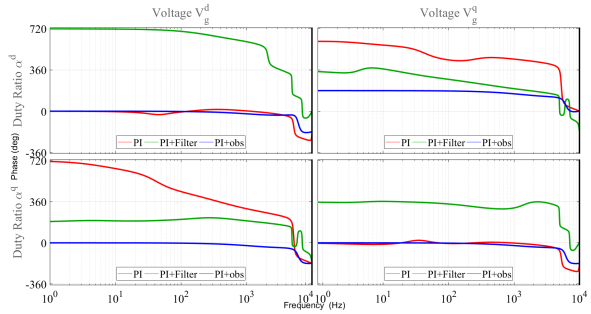

(b) Phase

Fig. 2. Bode diagram of the current controllers: traditional PI, PI with virtual impedances ("PI+filters") and PI with state observer ("PI+observer").

$$\begin{bmatrix} \hat{\overline{\boldsymbol{X}}} \\ \hat{\boldsymbol{\varepsilon}_{PI}} \end{bmatrix}^{+} = \begin{bmatrix} \overline{\boldsymbol{A}}^s + \boldsymbol{K}_p.\overline{\boldsymbol{B}}^s.\overline{\boldsymbol{C}}^s - \boldsymbol{L}.\overline{\boldsymbol{C}}^s & \boldsymbol{K}_i.\overline{\boldsymbol{B}}^s \\ \boldsymbol{K}_p.\overline{\boldsymbol{C}}^s & \mathbb{I}_{2,2} \end{bmatrix} . \begin{bmatrix} \hat{\overline{\boldsymbol{X}}} \\ \hat{\boldsymbol{\varepsilon}_{PI}} \end{bmatrix} + \begin{bmatrix} (\boldsymbol{K}_p + \boldsymbol{K}_i).\overline{\boldsymbol{B}}^s \\ \mathbb{I}_{2,2} \end{bmatrix} . \begin{bmatrix} i^d \\ i^q \end{bmatrix} + \begin{bmatrix} \boldsymbol{L} \\ \mathbb{O}_{2,2} \end{bmatrix} . \boldsymbol{Y}$$

$$\begin{bmatrix} \alpha^d \\ \alpha^q \end{bmatrix} = \frac{2.\left[\begin{bmatrix} \mathbb{O}_{2,2} & \mathbb{I}_{2,2} & \mathbb{O}_{2,4} \end{bmatrix} + \boldsymbol{K}_p.\overline{\boldsymbol{C}}^s \quad \boldsymbol{K}_i\right]}{V_{DC}} . \begin{bmatrix} \hat{\overline{\boldsymbol{X}}} \\ \hat{\boldsymbol{\varepsilon}_{PI}} \end{bmatrix} + \frac{2.(\boldsymbol{K}_p + \boldsymbol{K}_i)}{V_{DC}} . \begin{bmatrix} i^d \\ i^q \end{bmatrix} \quad (12)$$

D. Comparison Of The Controllers

The PI current controller, presented in (8), is compared with the PI controller integrating a state observer, presented in (12), as well as with a previous solution deployed in a VSG-based inverter at the Schneider Electric laboratory: a PI controller integrating stabilizing virtual impedances [17].

Fig. 2a and Fig. 2b present the three currents controllers, the traditional PI controller ("PI"), the PI controller with virtual impedances ("PI+filter") and the PI controller with a state observer ("PI+observer"), in bode diagrams. Magnitudes and phases, based on the input voltages V_g^d and V_g^q are proposed, considering the output controlled duty ratios α^d and α^q.

The magnitude characteristic, in Fig. 2a, show that the current controllers "PI" and "PI+filter" present similar magnitudes, with a high resonance peak at high frequencies. This resonance is reduced for the "PI+filter" thanks to the insertion

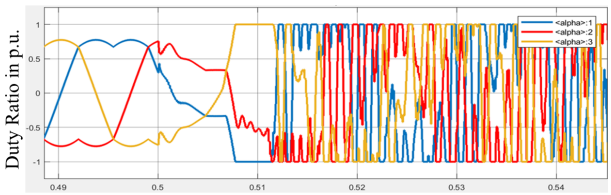

(a) PI

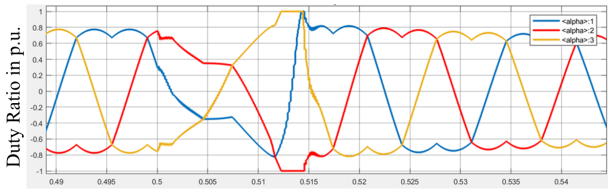

(b) PI+observer

Fig. 3. Traditional PI and PI with state observer ("PI+observer") inverter's duty ratios during a three-phase short-circuit (simulation).

of the virtual resistance, but remains nevertheless relatively important. The disadvantage of the high frequencies resonance peak is that it has a real impact on the stability of the system, especially during short circuits, which is a major disadvantage for these two controllers. The "PI+observer" possesses a quasi-constant magnitude characteristic. It can be noted that, thanks to the integration of the observer, the resonance peak is drastically reduced. Hence, the observer helps significantly stabilizing the current controllers.

On the phase characteristics of the current controllers, Fig. 2b, it can be noted that the phase shift for the "PI" and the "PI+filters" is important and can reach up to 720 °. The insertion of virtual impedances, in addition of consuming some power and decreasing the total efficiency, increases indeed significantly the phase shift between the inputs and the outputs. The phase shift of the "PI+observer" is mainly constant and close to zero. So, a major advantage of the integration of a state observer in the current controller is that it permits to mainly keep the phase shift between the voltages inputs and the controlled duty ratios constant and almost zero.

To conclude with this comparison, Fig. 2 illustrate the benefit of a state observer in the current controller in greatly stabilizing the system, especially during high frequencies phenomena as short-circuits, in addition to reduce the phase shift between the input voltages, V_g^d and V_g^q, and the output controlled duty ratios, α^d and α^q.

Fig. 3 represents the inverter's three phases duty ratios for both the PI and PI+observer controllers, during a three-phase short-short-circuit of 50 ms. As detailed in the Bode analysis, the PI controller is unstable during short-circuits and the addition of an observer stabilizes the response of the controlled system.

IV. Experimental Implementation

In this section, the advantage of the state observer integrated to the PI current controller for the VSG-based solution are experimentally validated.

A. Experimental Set-up

A power-in-the-loop (PHIL) approach has been used to validate the proposed solution as the transfer of the VSG-based control to another inverter requires significant costly material and human investments. To that purpose, in the facilities of the G2Elab, a laboratory-scale prototype has been built to develop and validate, for various scenarios, control strategies that enhance the capabilities of inverter-based generation systems notably used for renewable energies such as photovoltaic [19]–[21], wind turbines [22], [23] or microgrid controllers [24].

The test-bench is constituted of two main systems: the VSG-based inverter and the microgrid used to validate the portability of the control to another inverter. Each system can be divided in two layers: software and hardware. The software layer is also split in two: one for the inverter control and one for the emulated microgrid. Both are controlled and represented by their associated real-time digital simulators, dSPACE® and RT-LAB® respectively.

Due to the test-bench technical configuration, both simulators, dSPACE® and RT-LAB®, are simultaneously used, but at different frequencies. The emulated microgrid is controlled at a fixed frequency of 20 kHz and the VSG control (including the pulse width modulation switching frequency) have been tested for a frequency of 10 kHz.

The hardware part of the microgrid consists of a connection to the local distribution grid, real controllable loads (able to create unbalanced operation) and the power interface that controls the power amplifier, in turn used to emulate the microgrid. The emulated microgrid's model is developed using MATLAB®/Simulink® and then integrated in the RT-LAB® platform at a frequency of 20 kHz. The emulated microgrid contains traditional, industrial, nonlinear and unbalanced loads, two different power sources, a diesel engine generator and a VSG-based inverter. There is the possibility to create faulty conditions at the point of coupling to validate the real VSG-based inverter stability during a fault.

Fig. 4 presents the schematic diagram of the laboratory-scale PHIL prototype system put in place to validate and compare the VSG-based current controllers. It is constituted of:

- Real and emulated, balanced and unbalanced loads;
- Emulated industrial and nonlinear loads (for instance a 2 kVA induction motor);
- Other power sources: an emulated VSG of 4 kVA, an emulated generator of 4 kVA and the possible connection to the local distribution grid;
- Faults generation capabilities in both an emulated and a real microgrid.

B. Experimental Results

Fig. 5 shows the transient dynamic behavior of the VSG-based inverter under a resistive 20 kW load shedding with the PI controller integrating (Fig. 5b) or not (Fig. 5a) the state-space observer. The VSG-based inverter is supplying, at the inverter's maximal power, a 4 kW load. After 50 ms, the load

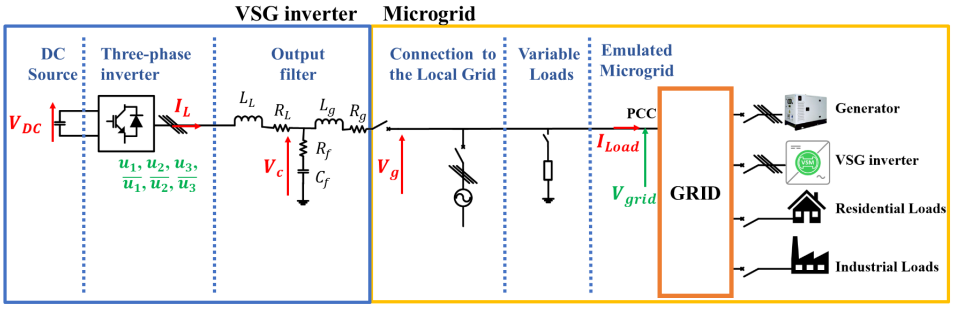

Fig. 4. Schematic diagram of the laboratory-scale PHIL prototype system put in place to validate VSG-based controllers.

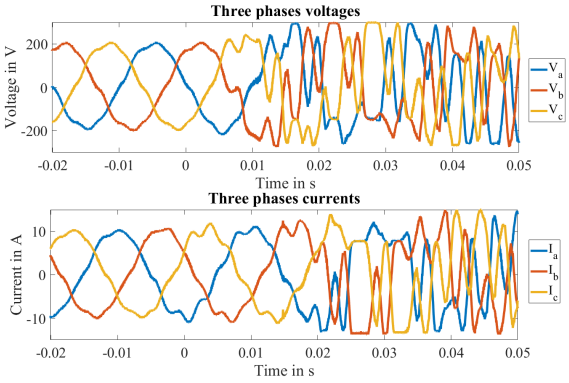

(a) "PI"

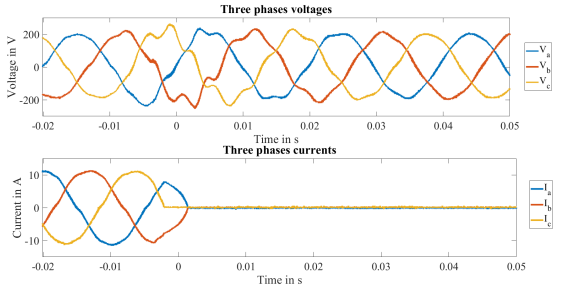

(b) "PI+observer"

Fig. 5. VSG three phase output voltages and currents during a load shedding.

is disconnected to simulate a large load shedding. Fig. 5a shows that the PI controller integrated in the VSG is unstable when the VSG is off-loaded, which constitute a major issue preventing its validation for future developments.

As the VSG mimics a synchronous machine, the operated range should be similar: loads ranging from 0 % to 100 % of apparent power. However, other tests (not proposed in this paper) were also conducted on the VSG in closed-loop with the PI controller, showing that the system is unstable if the load shed consume more than 70 % of the VSG active power or more than 30 % of the VSG reactive power. These phenomena are linked to the magnitude resonance peak that can be seen in Fig. 2a.

For information, this controller is also failing short-circuit tests. Indeed, during short-circuits, the saturation of the inverter is often reached. The problem is that, even after the disappearance of the short-circuit, the closed loop PI controller behavior cannot reach a stable state again. The main problem is in fact that the control does not take into account phenomena that can destabilize the closed-loop system [12].

On the contrary, Fig. 5b shows that the PI controller integrating a state observer is stable when the VSG is off-loaded in the same conditions. Thanks to the observer, minimizing the resonance peak, the perturbation due to the load shedding is rejected. The VSG-based inverter stays stable during and after the perturbation. The output current of the inverter is going from its nominal value, 10 A supplying a 4 kW load, to 0 A after the load shedding. The outputs voltage increases when the load is disconnected, but rapidly stabilizes, in less than a period, 0.02 ms, at its nominal value. Comparing Fig. 5b and Fig. 5a, the observer clearly stabilizes the system when submitted to this harsh event, which was anticipated based on the analysis of Fig. 2a. Other tests, not detailed in this paper, were also conducted on the VSG implementing the PI controller and the state observer: load impacts, highly inductive loads variations, unbalanced or non-linear loads, parallel operations as well as short-circuit. Thanks to the integration of the observer, the VSG remains stable during those tests in the microgrid represented in Fig. 4.

V. Conclusion

In this paper, a control architecture based on the state-space model, combined with an observer, is proposed to enhance the stability of an inverter-based generator operated as a virtual synchronous generator (VSG) in a microgrid. VSGs are submitted to sudden and almost unpredictable load variations at the microgrids level. Hence, the proposed controller has been designed as a solution to face the unpredictability of load consumption, thus decreasing risks of instability thanks to the integration of an observer.

First, the state-space model is expressed based on the grid-connected inverter. Second, the controller, including a state observer, of the VSG-based inverter is detailed. The addition of an observer allows the VSG solution to survive harsh events as it is analyzed with a Bode representation, in comparison with more traditional controllers (only a PI and a PI including virtual impedances as filter). Finally, the paper concludes with experimental results validating the relevance and the

robustness of the proposed control of the VSG. The current controller integrating a state observer is able to face a 100 % load impact as well as short-circuits. The stability of such solution is thus validated.

REFERENCES

[1] A. Hoke, R. Butler, J. Hambrick, and B. Kroposki, "Maximum Photovoltaic Penetration Levels on Typical Distribution Feeders," *IEEE Transactions on Sustainable Energy*, no. July, 2012.

[2] J. Driesen and K. Visscher, "Virtual synchronous generators," in *IEEE Power and Energy Society General Meeting - Conversion and Delivery of Electrical Energy in the 21st Century*, no. August 2008. Pittsburgh, USA: IEEE, Jul. 2008, pp. 1–3.

[3] R. Hesse, D. Turschner, and H.-P. Beck, "Micro grid stabilization using the virtual synchronous machine VISMA," in *International Conference on Renewable Energies and Power Quality*, 2009, pp. 15–17.

[4] H. Bevrani, T. Ise, and Y. Miura, "Virtual synchronous generators: A survey and new perspectives," *International Journal of Electrical Power and Energy Systems*, vol. 54, pp. 244–254, Jan. 2014.

[5] V. V. Thong, A. Woyte, M. Albu, M. V. Hest, J. Bozelie, J. Diaz, T. Loix, D. Stanculescu, and K. Visscher, "Virtual synchronous generator: Laboratory scale results and field demonstration," in *IEEE PowerTech*, Bucharest, Romania, 2009, pp. 2–7.

[6] Y. Chen, R. Hesse, D. Turschner, and H.-P. Beck, "Comparison of methods for implementing virtual synchronous machine on inverters," in *International Conference on Renewable Energies and Power Qualities*, vol. 1, no. 10, 2012, pp. 734–739.

[7] Q.-c. Zhong and G. Weiss, "Synchronverters: grid-friendly inverters that mimic synchronous generators," in *Control of Power Inverters in Renewable Energy and Smart Grid Integration*. Chichester, West Sussex, United Kingdom: John Wiley & Sons, Ltd., Nov. 2012, vol. 58, no. 4, pp. 277–296.

[8] Y. Hirase, K. Abe, K. Sugimoto, and Y. Shindo, "A grid-connected inverter with virtual synchronous generator model of algebraic type," *Electrical Engineering in Japan*, vol. 184, no. 4, pp. 10–21, Sep. 2013.

[9] K. Sakimoto, K. Sugimoto, and Y. Shindo, "Low voltage ride through capability of a grid connected inverter based on the virtual synchronous generator," in *IEEE International Conference on Power Electronics and Drive Systems (PEDS)*. IEEE, Apr. 2013, pp. 1066–1071.

[10] H. Zhao, H. Zeng, and Q. Yang, "Virtual synchronous generator based multi-loop control of renewable DGs in island microgrids," in *Chinese Control and Decision Conference (CCDC)*. IEEE, May 2016, pp. 423–428.

[11] D. J. Hogan, F. Gonzalez-Espin, J. G. Hayes, G. Lightbody, L. Albiol-Tendillo, and R. Foley, "Virtual synchronous-machine control of voltage-source converters in a low-voltage microgrid," in *European Conference on Power Electronics and Applications (EPE ECCE Europe)*. IEEE, Sep. 2016, pp. 1–10.

[12] H. Alatrash, A. Mensah, E. Mark, R. Amarin, and J. H. R. Enslin, "Generator emulation controls for photovoltaic inverters," in *International Conference on Power Electronics (ECCE Asia)*, vol. 3, no. 2. IEEE, May 2011, pp. 2043–2050.

[13] C. F. Dos Santos, F. B. Grigoletto, and M. Stefanello, "Power quality improvement in a grid connected voltage source inverter using the concept of virtual synchronous machine," in *IEEE Brazilian Power Electronics Conference and 1st Southern Power Electronics Conference (COBEP/SPEC)*. IEEE, Nov. 2015, pp. 1–5.

[14] M. Chen and X. Xiao, "Hierarchical frequency control strategy of hybrid droop/VSG-based islanded microgrids," *Electric Power Systems Research*, vol. 155, pp. 131–143, 2018.

[15] C. Andalib-Bin-Karim, X. Liang, and H. Zhang, "Fuzzy-Secondary-Controller-Based Virtual Synchronous Generator Control Scheme for Interfacing Inverters of Renewable Distributed Generation in Microgrids," *IEEE Transactions on Industry Applications*, vol. 54, no. 2, pp. 1047–1061, Mar. 2018.

[16] P. Kundur, *Power System Stability and Control*. New York: McGraw-Hill, 1994.

[17] M. A. Rahmani, Y. Herriot, S. L. Sanjuan, and L. Dorbais, "Virtual synchronous generators for microgrid stabilization : Modeling, implementation and experimental validation on a microgrid laboratory," in *Asian Conference on Energy, Power and Transportation Electrification (ACEPT)*, vol. 2017-Decem. IEEE, Oct. 2017, pp. 1–8.

[18] A. Pearson, "Linear optimal control systems," *IEEE Transactions on Automatic Control*, vol. 19, no. 5, pp. 631–632, Oct. 1974.

[19] L. Bun, B. Raison, G. Rostaing, S. Bacha, A. Rumeau, and A. Labonne, "Development of a real time photovoltaic simulator in normal and abnormal operations," in *Annual Conference of the IEEE Industrial Electronics Society (IECON)*. IEEE, Nov. 2011, pp. 867–872.

[20] A. Mercier, C. Benoit, Y. Besanger, A. Rumeau, and C. Boudinet, "Comparative study of solar panel decentralized controls in low voltage network with real time simulation," in *IEEE Power and Energy Society General Meeting*, 2015, iSSN 1944-9933.

[21] A. Ovalle, G. Ramos, S. Bacha, A. Hably, and A. Rumeau, "Decentralized control of voltage source converters in microgrids based on the application of instantaneous power theory," *IEEE Transactions on Industrial Electronics*, vol. 62, no. 2, pp. 1152–1162, 2015.

[22] A. Djoudi, S. Bacha, H. Chekireb, H. Iman-Eini, and C. Boudinet, "Adaptive Sensorless SM-DPC of DFIG-Based WECS under Disturbed Grid: Study and Experimental Results," *IEEE Transactions on Sustainable Energy*, vol. 9, no. 2, pp. 570–581, 2018.

[23] B. Guo, S. Bacha, M. Alamir, A. Mohamed, and C. Boudinet, "LADRC applied to variable speed micro-hydro plants: Experimental validation," *Control Engineering Practice*, vol. 85, no. February, pp. 290–298, Apr. 2019.

[24] Quang Linh Lam, "Advanced control of microgrids for frequency and voltage stability : robust control co-design and real-time validation," Ph.D. dissertation, Université Grenoble Alpes, 2018.

APPENDIX

$$\boldsymbol{A} = \omega_0. \begin{bmatrix} -\frac{R_L}{L_L} & \omega_r & -\frac{1}{L_L} & 0 & 0 & 0 \\ -\omega_r & -\frac{R_L}{L_L} & 0 & -\frac{1}{L_L} & 0 & 0 \\ \frac{1}{C_f} - \frac{R_f.R_g}{L_g} & 0 & -R_f.\left(\frac{1}{L_L}+\frac{1}{L_g}\right) & \omega_r & -\left(\frac{1}{C_f} - \frac{R_f.R_g}{L_g}\right) & 0 \\ 0 & \frac{1}{C_f} - \frac{R_f.R_g}{L_g} & \omega_r & -R_f.\left(\frac{1}{L_L}+\frac{1}{L_g}\right) & 0 & -\left(\frac{1}{C_f} - \frac{R_f.R_g}{L_g}\right) \\ 0 & 0 & \frac{1}{L_g} & 0 & -\frac{R_g}{L_g} & \omega_r \\ 0 & 0 & 0 & \frac{1}{L_g} & \omega_r & -\frac{R_g}{L_g} \end{bmatrix}$$

$$\boldsymbol{B} = \omega_0. \begin{bmatrix} \frac{V_{DC}}{2.L_L} & 0 \\ 0 & \frac{V_{DC}}{2.L_L} \\ \frac{R_f.V_{DC}}{2.L_L} & 0 \\ 0 & \frac{R_f.V_{DC}}{2.L_L} \\ 0 & 0 \\ 0 & 0 \end{bmatrix} ; \boldsymbol{C} = \omega_0. \begin{bmatrix} 0 & 0 \\ 0 & 0 \\ \frac{R_f}{L_g} & 0 \\ 0 & \frac{R_f}{L_g} \\ -\frac{1}{L_g} & 0 \\ 0 & -\frac{1}{L_g} \end{bmatrix}$$